Radio-magnetotelluric and controlled-source magnetotelluric surveys on a frozen lake: Opportunities for urban applications in Nordic countries

Mehrdad Bastani[1,2]*, Shunguo Wang[3], Alireza Malehmir[1] and Suman Mehta[4]

[1]*Department of Earth Sciences, Uppsala University, Uppsala, SE-75236, Sweden,* [2]*Geological Survey of Sweden, Box 670, Uppsala, SE-75128, Sweden,* [3]*Department of Electronic Systems, Norwegian University of Science and Technology, NO-7491, Trondheim, Norway, and* [4]*AAC Clyde Space, Uppsala Science Park, SE-751 83, Uppsala, Swedan*

ABSTRACT

In a novel approach, we have carried out controlled-source and radio-magnetotelluric measurements in the frequency range of 2–250 kHz on a frozen lake located over a planned major multi-lane underground road tunnel near the city of Stockholm. The aim was to gain a better understanding of the resistivity variations above and, potentially, within the crystalline bedrock. Previous studies on the lake water using the boat-towed radio-magnetotelluric technique at the higher end of the frequency band lacked resolution at depth and could not provide conclusive information about bedrock level and potential fracture systems within the bedrock. Taking advantage of Nordic winters, we measured four profiles on the frozen lake complementing the previously acquired boat-towed radio-magnetotelluric data utilizing a double horizontal magnetic dipole transmitter that generated signals down to 1 kHz. The new resistivity models, incorporating the lower frequency data, show improvements and deeper penetrations based on a combined analysis of penetration depth, data misfits and sensitivity studies. The resistivity models also show better correlation with the available high-resolution shallow water seismic reflection data and the geological observations. A potential fracture system within the bedrock can also be inferred better in the new models. The idea of running similar surveys on frozen lakes can be further exploited in similar conditions in countries such as Sweden, where approximately 7% of the land is covered by freshwater bodies and poorly explored for infrastructure planning projects.

Key words: Electromagnetic, resistivity, shallow subsurface, Tunnel.

INTRODUCTION

It is common practice to plan high-resolution surface geophysical measurements in areas suggested by either interpretation of airborne data or other disciplines involved in a project, for example geo-technicians or mine engineers. One of the challenges in planning such surveys is sometimes the presence of waterbodies, such as lakes and rivers, which may cross or cover the target structures. One such example is the 21-km-long Stockholm Bypass in Sweden, where 18 km is below the ground surface and planned as two separate tunnels, each having three lanes. The tunnels at three locations pass under Lake Mälaren (Fig. 1). Luckily, in such areas, the cold winters furnishes the possibility of running geophysical measurements on frozen waterbodies. Geophysical measurements on frozen lakes and seas have been

*E-mail: mehrdad.bastani@sgu.se

Figure 1 Location of the study area. (a) The Stockholm Bypass (Förb-ifart) project. The planned bypass is shown with the green track. (b) Profile section of water passages, marked by numbers 1 to 3, showing the location and depths to the top of the tunnel. The inset map in (a) shows the location of the study area in Sweden.

carried out over the past decades for various purposes. Gravity measurements on the surface of frozen lakes in northern parts of Europe (mainly Scandinavia) and North America are routinely conducted over the winter periods. Ugalde *et al*. (2006) collect gravity data at 98 stations over the frozen Wanapitei Lake in Sudbury, northern Ontario, Canada. Inclusion of the collected data into the existing database improved the

Bouguer anomaly map in resolving the extent of a known meteorite crater below the central parts of the lake. Andersson and Malehmir (2018) conducted a similar survey in Sweden to find the lateral extent of a carbonatite system into the Baltic Sea. Dugan *et al*. (2016) report the use of ground penetrating radar (GPR) to study small-scale structures within the ice covering two lakes in McMurdo Dry Valleys, Antarctica. Their findings confirmed the results from an earlier study carried out in Lake Vida, where airborne transient electromagnetic data were also collected and modelled (Dugan *et al*. 2015, and reference therein). Schwamborn et al. (2002) collected high-resolution seismic reflection and GPR data over Lake Niko-lay in the western Lena Delta to study the uppermost basin fill and the bordering of frozen margins. Their results showed that the combination of the two profiling systems provided detailed information about stratigraphy along the profiles in both frozen and unfrozen parts of the lake.

Radio-magnetotelluric (RMT) is an established electromagnetic (EM) method for mapping near-surface resistivity variations (Tuberg et al. 1994; Tezkan *et al*. 2000; Bastani 2001; Persson 2001; Bastani et al. 2012). The passive sources, such as very low frequency (VLF) and LF transmitters as well as a portable data acquisition system, make the RMT method an efficient and practical tool for near-surface geophysical surveys. However, acquiring RMT data over shallow waterbodies poses a challenge in many conditions and in particular in Scandinavia, where a considerable portion of the land is covered by waterbodies such as rivers and lakes. To overcome some of these challenges, a new acquisition technique called boat-towed RMT was introduced by Bastani *et al*. (2015), including an example of data acquisition over the freshwater body of Lake Mälaren in the outskirts of the city of Stockholm, Sweden, over the water passages where the tunnels of Stockholm Bypass cross. The EnviroMT instrument (Bastani 2001) was modified to carry out the waterborne RMT survey. The analogue sensors were made to float on a wooden platform and towed by a boat at low speeds (0.5–1 m/s). The boat-towed acquisition system works effectively and is highly cost-effective. Mehta *et al*. (2017) examined and provided a detailed analysis of the resolution of boat-towed RMT data. Given the frequency range of the RMT data (10–250 kHz), it was evident that the RMT data acquired over Lake Mälaren provided better resolution at shallow depths compared to VLF data in the range of 10–30 kHz. However, a major drawback of the RMT system is that it works in a narrow frequency band, which limits the penetration depth . This limitation becomes more problematic in the presence of a conductive water column or sediments, which can for example hinder the

delineation of bedrock level and potential weakness zones within it, both of which have significant implications for the planning of underground infrastructures, reinforcements used and excavation methods (Malehmir et al. 2015; Dehghannejad et al. 2017).

In a recent study by Wang *et al.* (2018), boat-towed RMT data and lake-floor electrical resistivity tomography (ERT) are jointly inverted to model the structures below the waterbody at the Äspö Hard Rock Laboratory (HRL) site in southeastern Sweden. The resistivity models from the 2D inversions delineated subsurface structures, such as a major northeasterly directed fracture system that is highly saturated with saline water. The presence of a fracture zone is observed in the HRL underground facility and also confirmed by boreholes. The limited depth penetration of the RMT data is somehow compensated for in the inversion process by incorporation of the ERT data that are acquired with a reasonably long array extent (Ronczka *et al.* 2017).

Employing controlled-source audio magnetotelluric (CSAMT) at lower frequencies in the range 1–10 kHz is a proper solution to increase the penetration depth and for a reasonably fast data acquisition. The concept of controlled sources in magnetotelluric studies was originally developed to improve the signal strength (Goldstein and Strangway 1975), especially in areas close to manmade infrastructures where the background noise level is considerably high. In the controlled-source measurements, in order to meet the plane-wave approximation, the source, which is either an electric or magnetic dipole, should be sufficiently far enough from the measuring site. Zong and Hughes (1991) give a detailed account on the CSAMT method and discuss the conditions for near- and far-field electromagnetic data acquisition and interpretations. Wannamaker (1997) provides prerequisites for source–receiver separation to be 5 times the skin depth in order to avoid near-field effects (NFE). Pedersen *et al.* (2005) and Bastani et al. (2009, 2011) present the results of RMT and CSAMT measurements for a number of near-surface investigations. Sterich and Becken (2010) provide a detailed account on the EM fields from a finite-length wire source and compare it with a point dipole solution. They discuss the issues caused by the point source approximation, where hundreds of metres long wires are used to generate the EM signals. Use of controlled-source EM approaches for hydrocarbon exploration is discussed in detail by Streich (2016). Saraev et al. (2017) present the use of controlled-source radiomagnetotellurics (CSRMT) for near-surface investigations in remote regions. They demonstrate the use of a grounded electric dipole as a source, where they could measure the signal in a wide frequency range by utilizing the odd harmonics of the base frequency. Shlykov and Saraev (2015) discuss and present the possibilities of estimating the macro-anisotropy of the earth material from the RMT sounding and using a controlled source that transmits the signals up to 1000 kHz. They also provide a forward modelling solution that takes into account the displacement currents. Tezkan *et al.* (2019) show an application of the CSRMT survey to detect and model the buried faults in 2D in the Vuoska region, close to the city of St. Petersburg. The study included CSRMT measurements made using a horizontal electrical dipole using the frequencies of 0.5, 11.5, 30 and 105 kHz and their odd harmonics. They could successfully resolve and map the buried faults by using resistivity model from the 2D inversion of the acquired CSRMT data. Synthetic analysis carried out by Mehta *et al.* (2017) suggests that EM frequencies as low as 2.5 kHz should provide the desired penetration depth in the case of Lake Mälaren site to gain a better understanding of the fracture systems in the underlying resistive bedrock. The logistical requirement to acquire CSAMT data on shallow waterbodies with a floating platform is possible, but challenging, and can be time-consuming since the measurement time at each station can take a few minutes. To keep the towed platform with sensors stable at a location can also be difficult and impractical in places where ships and boats can pass often and frequently. Wang *et al.* (2019) present the results of their study at HRL site made in June 2017. They acquired boat-towed RMT and CSAMT data along a 600-m-long profile to showcase the increased penetration depth when the lower frequency data in the 1.25–12.5 kHz range are included in the 2D inversions. The resulting resistivity models resolve the deeper parts of the underlying fractured granite when compared to the inversion of just the RMT data. However, in the presented case, the measurement platform is stationary and stabilized during the data acquisition using a rope that is fixed to an island located in the middle of the profile. Such a procedure slows the production rate and might not be possible in many locations. Recently, Shlykov *et al.* (2020) present an interesting application of the CSRMT method to map and model permafrost in an area located at northern part of Siberia. By using the same data frequency range as presented in Tezkan *et al.* (2019), they could successfully delineate loam and sand horizons using the resistivity models from the 2D inversion of the CSRMT where they also compared the results with the existing borehole data. Yavich *et al.* (2020) present a new fast 3D parallel simulation code applied to the CSRMT data acquired in the Aleksandrovka study area in Kaluga Region, Russia. Their results reveal that the developed
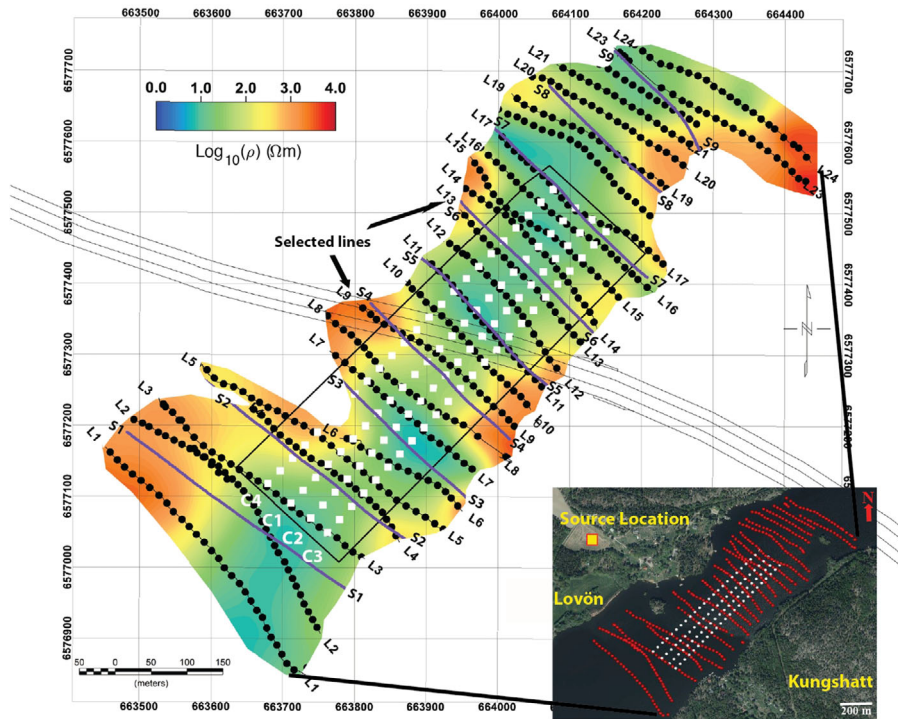
Figure 2 Location of the boat-towed RMT profiles (marked from L1 to L24 with black circles and lines) and the new CSRMT profiles (marked from C1 to C4 with white rhombus). In the background, the resistivity slice at 38 m depth from the 2D inversion of boat-towed RMT data is shown (Mehta *et al*. 2017). In the present study and to showcase the improvements, we used L9 RMT profile (marked with arrow) along with the four controlled-source stations that located along it. The location of the CSRMT source is shown in the inset figure (bottom right) with respect to the previously acquired RMT and the newly acquired CSRMT stations.

method can be applied in the very complex geological structures. In our case study, after a number of careful inspections, we took advantage of the Nordic winters and carried out the simultaneous RMT and CSAMT measurements on the frozen lake of Mälaren during February 2017. Hereafter we use the term CSRMT wherever the results from the combination of both methods are presented to make the text more compact and easier to follow, unless the RMT and CSAMT should separately be discussed.

The present study provides detailed information about the field procedures, source setup and data processing of the CSRMT measurements made for the first time on a frozen lake along four parallel profiles. The 2D inversion results of the acquired CSRMT data demonstrate deeper penetration, down to approximately 40–80 m depth, leading to a better delineation of the level and possible weakness zones within the resistive granitic bedrock, where the underwater planned tunnels will be running through. The resistivity models from 2D inversion also better correspond with the existing marine high-resolution reflection seismic data from the

same site illustrating the accuracy and effectiveness of the approach.

STUDY AREA AND SURVEY SETUP

The study area is located close to the city of Stockholm, Sweden. The measurements were carried out over one of the three water passages (Fig. 1) reported by Bastani *et al*. (2015). A detailed account of the geology in the area is given by Mehta *et al*. (2017). The selected water passage, number 2, is between the Lovön and Kungshatt islands (Fig. 1). The bedrock at the tunnel location is of granitic and partly metasedimentary rock types. Geological observations indicate fractures in the crystalline bedrock that vary in width (1–5 m) and are partly filled with clay, graphite and chlorite. The controlled-source radio-magnetotellurics data were collected along four profiles (Fig. 2) on the frozen Lake Mälaren. All the four profiles are nearly parallel to each other and run in a SW–NE direction. The distance between the profiles is approximately 50 m, with station interval of 25 m and 24 stations per profile
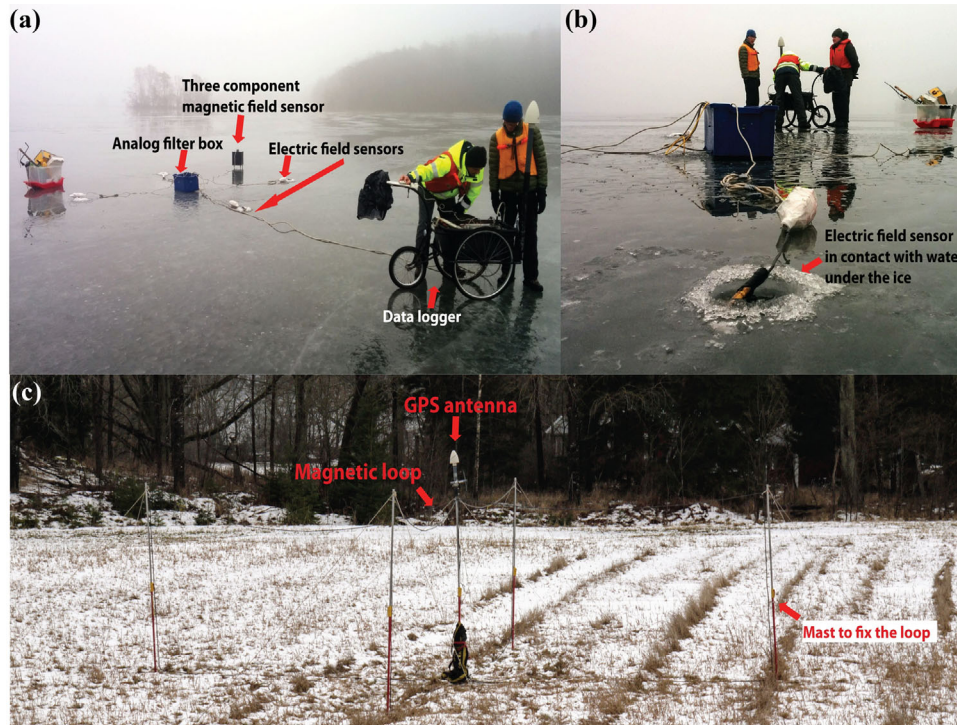
Figure 3 (a) Photo showing the EnviroMT CSRMT field setup while measuring on the Lake Mälaren near the city of Stockholm, Sweden. Different components of the setup are also shown. (b) A close look at the drill hole made in the ice crust for proper electric electrode contact with water. (c) The setup of the double magnetic dipole transmitter was used as source.

(a total length of ∼580 m). The frozen ice crust was about 10–15 cm at the time of the survey. Five holes were drilled to allow electrodes in contact with the lake water (one for grounding and four for two electric components). These holes (in total 500) were drilled using a handheld auger prior to the survey in order to allow faster station deployment.

DATA PROCESSING AND QUALITY

The EnviroMT (Bastani 2001) acquisition system was used to measure the electromagnetic (EM) signal. The setup of the EnviroMT field equipment is similar to a typical MT setup, as shown in Figure 3. The magnetic sensor is composed of three induction coils and is placed in such a way that the two horizontal sensors measure the magnetic field components along and perpendicular to the profile, while a third sensor measures the vertical component. Two pairs of electric field sensors and the horizontal magnetic field sensors are aligned either parallel or perpendicular to the profile direction. The system acquires data in two modes, namely radio-magnetotelluric (RMT) and controlled-source audio magnetotelluric (CSAMT). At each station, the RMT data in the frequency range 14–250 kHz

are acquired and stored first. Seven frequencies are used after the processing, and the transmitters during the acquisition are typically more than 20. Then the controlled-source signals, generated in the frequency range of 2.5–12.5 kHz, are recorded. In each measurement mode the data quality can be checked and, if necessary, the data at given mode/frequencies are repeated. The recorded data are the components of the EM field that are processed to estimate the complex-valued EM transfer functions, namely impedance tensor, **Z**, defined as:

$$\begin{bmatrix} E_x \\ E_y \end{bmatrix} = \begin{bmatrix} Z_{xx} & Z_{xy} \\ Z_{yx} & Z_{yy} \end{bmatrix} \begin{bmatrix} H_x \\ H_y \end{bmatrix} = \mathbf{Z} \begin{bmatrix} H_x \\ H_y \end{bmatrix} \tag{1}$$

and tipper vector (also referred to as vertical magnetic transfer function), **T,** given by:

$$H_z = \begin{bmatrix} T_x & T_y \end{bmatrix} \begin{bmatrix} H_x \\ H_y \end{bmatrix} = \mathbf{T} \begin{bmatrix} H_x \\ H_y \end{bmatrix} \tag{2}$$

where, E and H are the electric and magnetic field components, respectively. The subscripts x and y refer to directions of the sensors' setup in the field. In our case, x was perpendicular and y in the profile direction. In the routine MT data interpretation, the input data for forward modelling and inversion
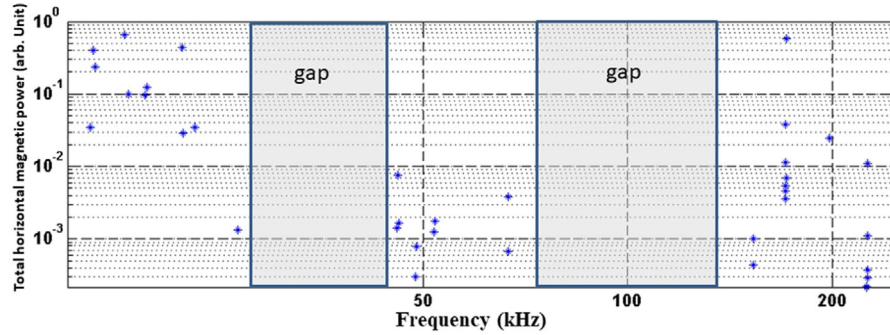
Figure 4 Amplitude of the power spectra (unit is arbitrary) of radio transmitters at station 6 profile 1. The grey boxes show the gaps in the RMT frequency range.

are the tipper data calculated as in equation (2), apparent resistivity and the impedance phase at a given target frequency, f, in measurement directions, xy or yx, calculated as:

$$\rho_{xy/yx}(f) = \frac{|Z_{xy/yx}|^2}{2\pi\mu_0 f} \tag{3}$$

$$\varphi_{xy/yx}(f) = \mathrm{Arg}(Z_{xy/yx}) \tag{4}$$

where xy refers to the electric field in the x direction and the magnetic field in the y direction, vice versa for yx.

The field data processing schemes integrated into the EnviroMT are detailed in Bastani (2001). In the RMT mode, at every station the number of selected transmitters depends on the site location and a predefined signal-to-noise ratio (S/N) of the total horizontal magnetic field power. For the Lake Mälaren survey, we used a threshold of 10 dB, and, on average, 24 radio transmitters were selected. The stored raw data are the mean stacked auto and cross powers of five components of the measured EM fields at selected transmitter frequencies. The RMT transfer functions (**Z** and **T**) are then estimated using the band-averaging technique (Bastani 2001). The uneven distribution and lack of radio transmitters in certain frequency bands affect the quality of the estimated transfer functions. Pederson et al. (2006) report gaps in the spectrum of radio transmitters in Europe. At the Lake Mälaren site, we could observe these gaps. Two such gaps are visible in the data (Fig. 4).

The signal source for the CSAMT measurements consists of two orthogonal horizontal magnetic dipoles. The source can remotely be controlled from the recording point. The location of the source is shown in Figure 2 with a yellow square mark. Based on the results of previous studies (Mehta et al. 2017), we selected five source frequencies of 2.5, 3.2, 5.0, 8.0 and 10 kHz. The source, when triggered, activates one of the

magnetic dipoles, and the signal is transmitted according to the given list of frequencies. The second dipole is then activated, and the same procedure is repeated (Bastani 2001). Eventually, the tensor transfer functions and their corresponding errors are estimated with a method given by Li and Pedersen (1991). As is also discussed by Li and Pedersen (1991), at certain distances from the transmitter site the data might contain EM signals that are not only dependent on the induced currents in the earth electrical resistivity structure, but also depend on the type of the transmitter/source used. At large distances, where the penetration depth of EM signal is considerably smaller (5–10 times) than the distance to the source, the wave can be considered as a plane and the source effects are negligible. In the RMT case, the EM waves are certainly plane, and the data can be inverted using the standard 2D/3D MT programs. However, for the inversion of combined RMT and CSAMT data, one must ascertain that the latter are measured at distances large enough from the source where the plane-wave assumption is met. At closer distances/lower frequencies, the source effects might be either considered (using a code that takes the source effects into account; for example see Wang et al. 2019) or the source contaminated data, namely near-field data, must be rejected prior to the inversion.

The data collected in our study show a smooth transition between the RMT and CSAMT frequencies in both apparent resistivity and phase data. This provides an indication of CSAMT data being in the far field. The typical signature of the near-field effect for a magnetic dipole source in the case of a homogeneous half space is that, with decreasing frequency, the phase rises above 45 degrees and apparent resistivity decreases. In this study, the closest and farthest stations to the source were at distances 477 m and 625 m, respectively, and the second closest station is 516 m away from the source. At a few stations on the northwestern part of the area, some
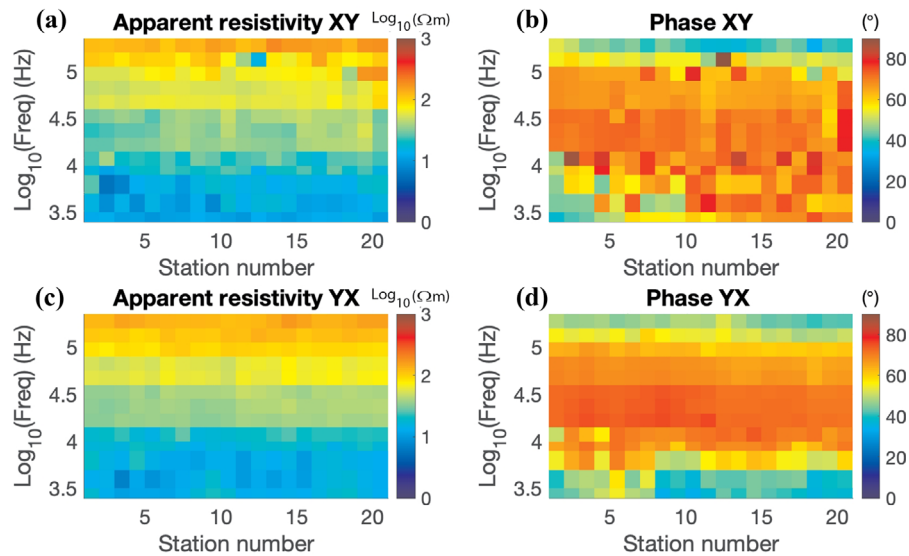
Figure 5 Measured apparent resistivity and phase of CSRMT data at stations along profile C1. (a) Apparent resistivity in the *XY* direction, (b) phase in the *XY* direction, (c) apparent resistivity in the *YX* direction, (d) phase in the *YX* direction. At most stations the transition between RMT and controlled-source data is smooth.

signs of the near-field effects (NFE) were observed in the raw data at lower frequencies. Most of the measuring stations located at a distance greater than 500 m from the source did not show any NFE. An example of raw data quality along profile C1 is shown in Figure 5. A smooth transition from the RMT to CSAMT frequencies provides confidence when combining both datasets for further modelling and interpretation. The controlled-source data in the *YX* direction show more sensitivity in detecting a resistive structure at the deepest parts of the profile as compared to data in the *YX* direction. Especially, a decreasing phase in the *YX* direction from values >55 degrees to values below 45 degrees along almost the entire profile indicates the presence of a resistive structure at depth. The phase in the *XY* direction shows a similar trend at the starting stations (1–10) and no sensitivity along the rest of the profile. The apparent resistivity data do not show clear indication of a resistive feature at the lowest frequencies.

2D inversion of combined radio-magnetotelluric and controlled-source radio-magnetotelluric data

As mentioned earlier, the most important objective when acquiring the controlled-source radio-magnetotelluric (CSRMT) data in the area (Fig. 1) was to increase the depth of penetration using lower frequencies to the level where the planned tunnels would be excavated. The CSRMT profiles are perpendicular to the boat-towed radio-magnetotelluric (RMT) profiles (Bastani *et al.* 2015; Mehta *et al.* 2017) and cover the

area with the deepest water column where the RMT signal may not reach the crystalline bedrock. This means that the measured CSAMT data can be included in the inversion of the boat-towed RMT data to improve sensitivity to the resistivity variations within the bedrock. We used the EMILIA program (Siripunvaraporn and Egbert 2000; Kalscheuer *et al.* 2008) for the 2D inversion of the CSRMT data, which uses the finite difference method for forward solver and Gauss–Newton method for the inversion. Mehta *et al.* (2017) carried out strike and dimensionality analysis for the previously acquired RMT data and showed that the geological strike is along the water passage, nearly perpendicular to the RMT profiles. Thus, no rotation of the data collected in both campaigns was required. Joint transverse electric (TE) and transverse magnetic (TM) mode inversions, namely TE + TM, were carried out on the CSRMT dataset to obtain a better constraint on the deeper parts of the models (Pedersen and Engels 2005). In the TE mode, electric current flows along the strike direction. In the TM mode, the electric current flows in the plane perpendicular to the strike direction. An error floor of 10% on the apparent resistivity and 5% ($\sim$2.86°) on the phase was used in the inversion. The design of the model mesh was such that the shallowest block size was 0.5 m thick, and the subsequent cell thickness increased with a geometrical progression factor of 1.12. The deepest cell thickness was 2500 m. We considered two blocks per measuring point for the horizontal dimensions of cells. We used a homogeneous half space of 1000 Ωm as the starting model. Regularization is used for smoothness

constraint in the inversion (Constable *et al.* 1987). The horizontal smoothness weighting factor is equal to the vertical one, so that no preferred smoothness was given in any direction.

The selected boat-towed RMT profile L9 (marked with an arrow in Fig. 2) coincides with four controlled-source stations. These two datasets were combined and inverted together. The inversion was carried out with two steps: (1) the Occam inversion with the maximal data inclusion unless the data point is too noisy to be accepted and (2) the damped Occam inversion with the data points which have reasonable misfits. In the second step, the starting model is the best-fitted model in the first inversion. More details can be found in Wang *et al.* (2018). Besides, two lowest frequencies (2.5 and 3.2 kHz) at the station closest to the source were omitted to eliminate the near-field effects. For a conservative consideration, the distance between the source and receivers is required to be 12 times larger than the skin depth to avoid the near-field effect. Figure 6(a) shows the resistivity model from joint inversion of TE + TM mode of only RMT data (boat-towed) along L9 (see, Fig. 2 for the location) with a root mean square (RMS) of 1.74. Figure 6(b) shows the results from the combined RMT and CSAMT datasets with an RMS of 1.62. The detailed data misfits are also shown in Figure 7. TE-mode apparent resistivities have a relatively high misfit at 28.31 kHz in the middle of the profile, while TM-mode apparent resistivities have a relatively high misfit at 226.50, 160.03 and 28.31 kHz in the middle of the profile. However, the phase data in both modes have low misfits. The inverse model has shallow structures well constrained by RMT data and deeper structures constrained by CSAMT data (Fig. 6). The major difference in the two models is in the middle of the profile, where a resistive feature below the conductive layer can be more clearly observed when the CSAMT data are included. The controlled-source data at stations located in the middle of the profile, where the conductive marine sediments overlying the more resistive and partly fractured crystalline have likely the greatest thickness, show considerable improvement in the model resolution at depth thanks to the increased penetration depth. The penetration depth, white dashed lines in Figure 6, was calculated as 1.5 times skin depth based on Spies (1989) and Huang (2005). The feature in the model below the penetration depth is not reliable for interpretation.

Seismic reflection data

The seismic reflection data were acquired in a separate project and by another party (Nilsson 2008). However, data in the form of raw shot gathers were made available to us for comparative studies and supporting the current studies. The dataset covers the two water passages and was acquired over the planned tunnels using a 12-channel hydrophone-streamer system positioned 0.5 m in the water. Hydrophones were separated by 1 m. A boomer was used as the seismic source. A sampling rate of 0.125 ms was used for the acquisition. The reflection data processing involved mainly marine geometry setup, velocity analysis and stacking. No migration was attempted since the dataset is quite shallow and that diffractions likely from undulated bedrock or fractured bedrocks were intended to be kept for interpretations. Multiples, while strong from both the lake floor (sediments) and bedrock, did not influence this study as the target depths were only a few metres into the bedrock and the multiples arrived much later in the dataset. The water bottom and base sediment reflections can clearly be seen in the seismic reflection section (Fig. 6c). Only two sections (S4 and S6) are presented together with CSRMT results in this study since the main objective is to investigate the CSRMT survey results.

INTERPRETATION AND DISCUSSION

The resistivity model obtained from the 2D inversion of only radio-magnetotelluric (RMT) dataset shows some distinct resistive features (Fig. 6a). The shallowest part of the model, mainly in the form of a 10–12 m thick layer with a resistivity of ∼200 Ωm, represents the freshwater. The large contrast between the freshwater resistivity and the underlying lake sediments with considerably lower resistivity yields the best-case scenario for the inversion to resolve the boundaries between the two, especially with the inclusion of controlled-source audio magnetotelluric (CSAMT) data (Fig. 6b). The water-sediment boundary also well corresponds with the strong reflection seen in the reflection seismic data (Fig. 6c). The underlying, more conductive lake sediments layer has a varying thickness along the profile that seems to be generally thinner on the NW and SE ends and thicker in the central part of the water passage. This limits the depth penetration of the RMT signal and leads to the ambiguities when analysing the bedrock resistivity variations using just the RMT resistivity models. However, the CSAMT data, with lower frequencies, are better at resolving the features in the bedrock.

Information available from a few cored boreholes in the area suggests the presence of fracture systems with a varying width of a few centimetres to tens of centimetres within the bedrock, and the total width of the fracture systems can reach up to 1–5 m (Ignea 2015; Mehta *et al.* 2017). The dominant
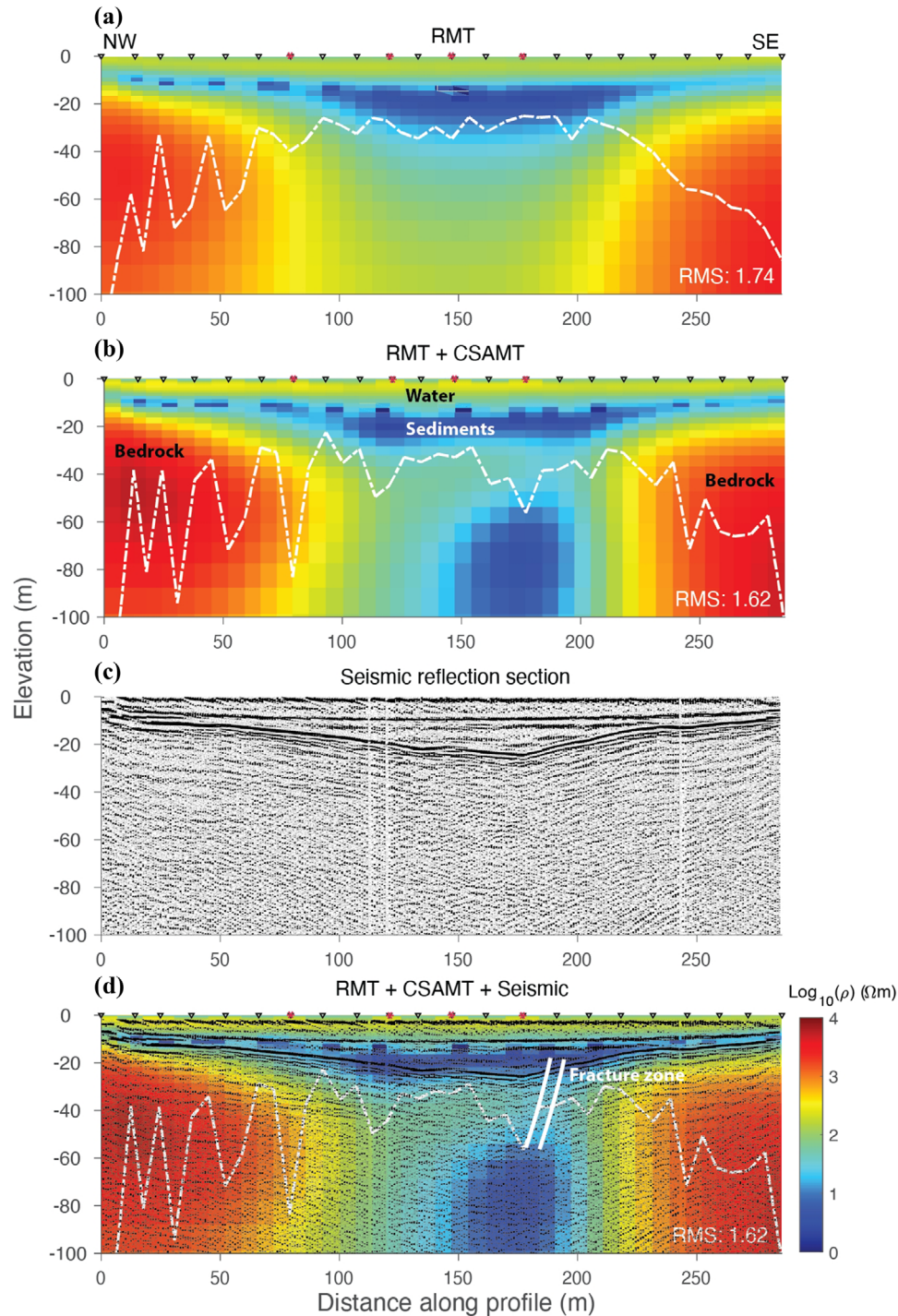
Figure 6 2D inversion models of (a) RMT and (b) combined RMT and CSAMT dataset from L9 line shown in Figure 1. The location of the controlled-source stations along the profile is marked by red '*' in (b), and the location of RMT station is marked by inverse triangles. (c) For comparison, a nearly collocated reflection seismic section along the resistivity profile is superimposed (d) into the model shown in (b). The improvement is significant especially in better delineating bedrock level and its undulation on the middle part of the profile. Penetration depth of data is marked in white dashed line, and the potential fracture zone is marked in white line.
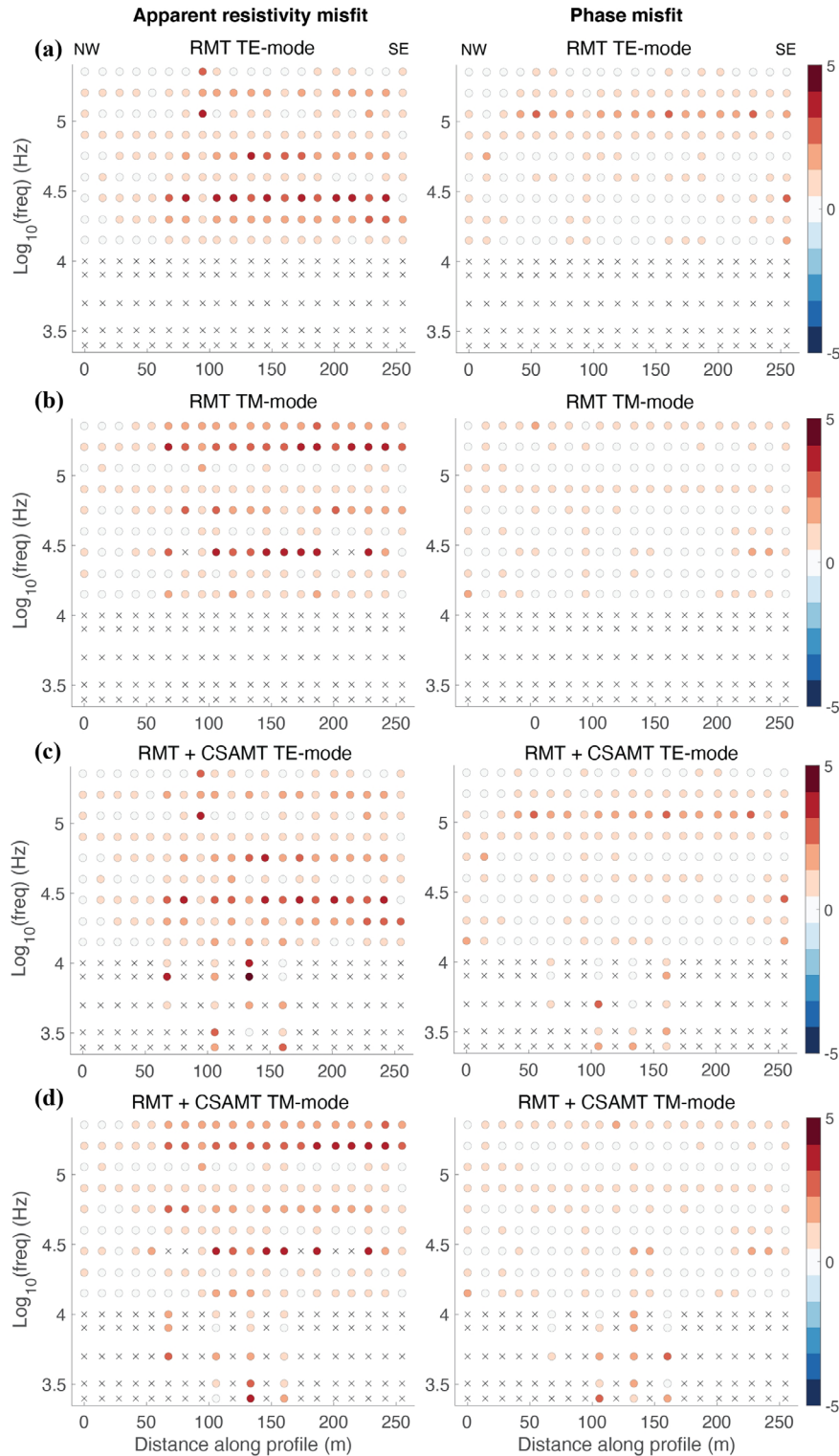
Figure 7 Data misfits corresponding the inversion in Fig. 6, which are the observed and modelled data difference normalized by the data errors. In general, phase data have lower misfits than the apparent resistivity data. The crosses mean the exclusion of data points in the corresponding inversions.
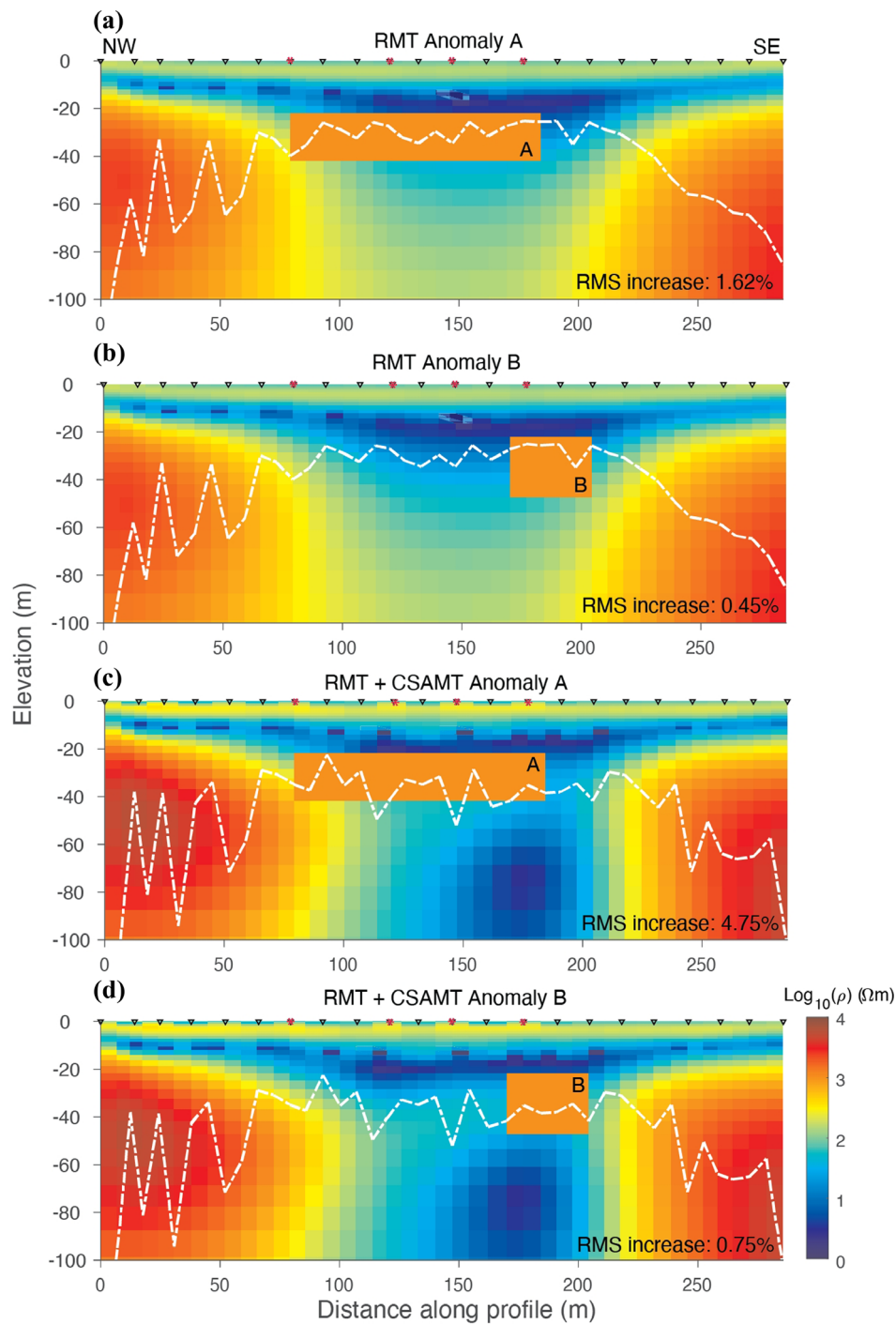
Figure 8 Sensitivity test of anomaly A and anomaly B. The resistivity of the anomalies is increased to 1000 Ωm from the inverted values for model perturbation. The RMS increase is the original and perturbed RMS difference normalized by the original RMS. (a) Anomaly A for RMT inversion, (b) anomaly B for RMT inversion, (c) anomaly A for RMT plus CSAMT inversion, and (d) anomaly B for RMT plus CSAMT inversion. The RMS increases of RMT plus CSAMT inversions are about 2–3 times larger than those of RMT inversions, which indicates the increase of sensitivity at depths due to the inclusion of four CSAMT stations.
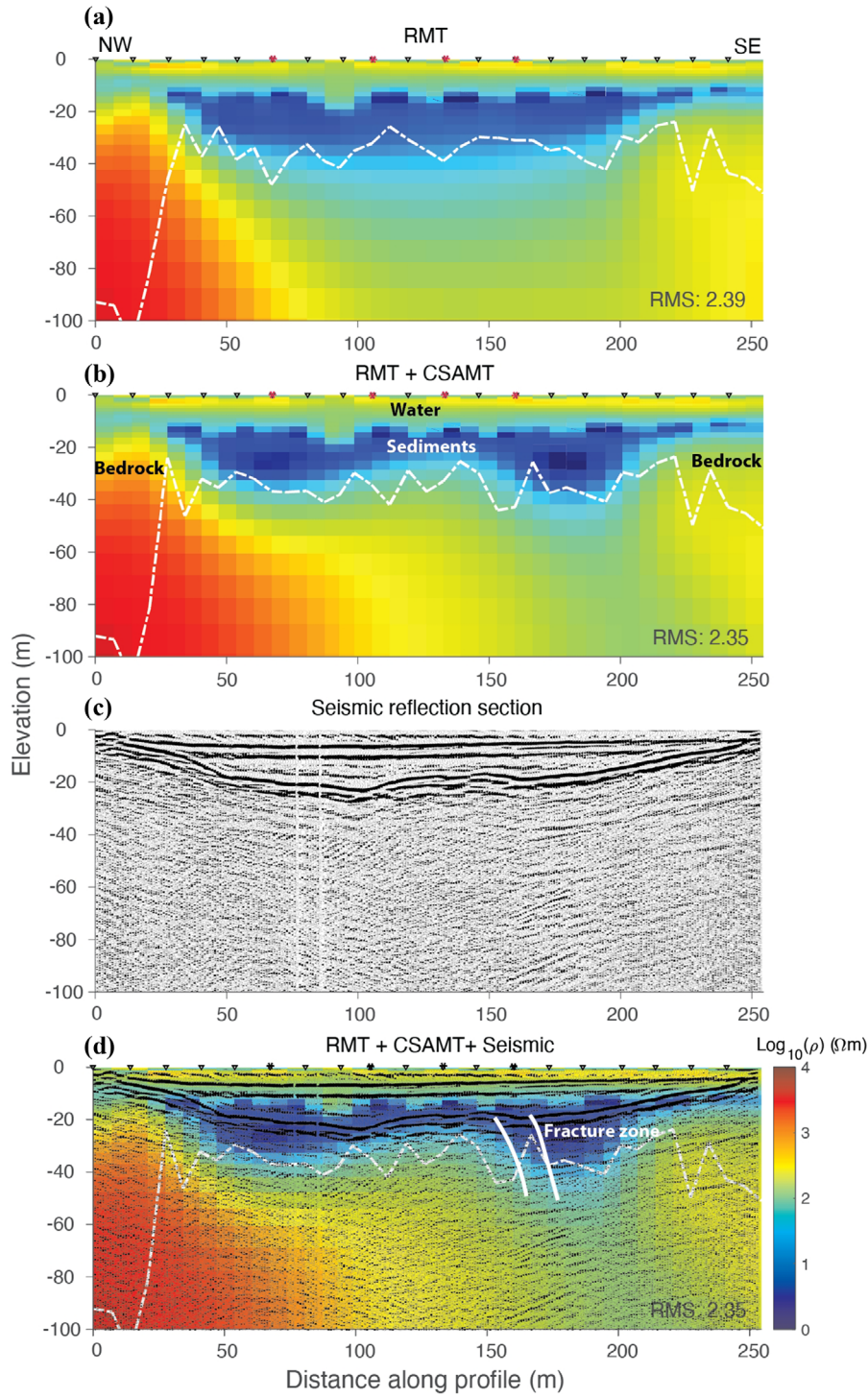
Figure 9 2D inversion models of (a) RMT and (b) combined RMT and CSRMT dataset from the L13 line shown (see Fig. 2 for locations) and the location of the controlled-source stations along the profile is marked by red '*' . (c) Reflection seismic data along the same profile. (d) For comparison, the nearly collocated reflection seismic section along the resistivity profile is superimposed on the resistivity model shown in (b). Penetration depth of data is marked in white dashed line.
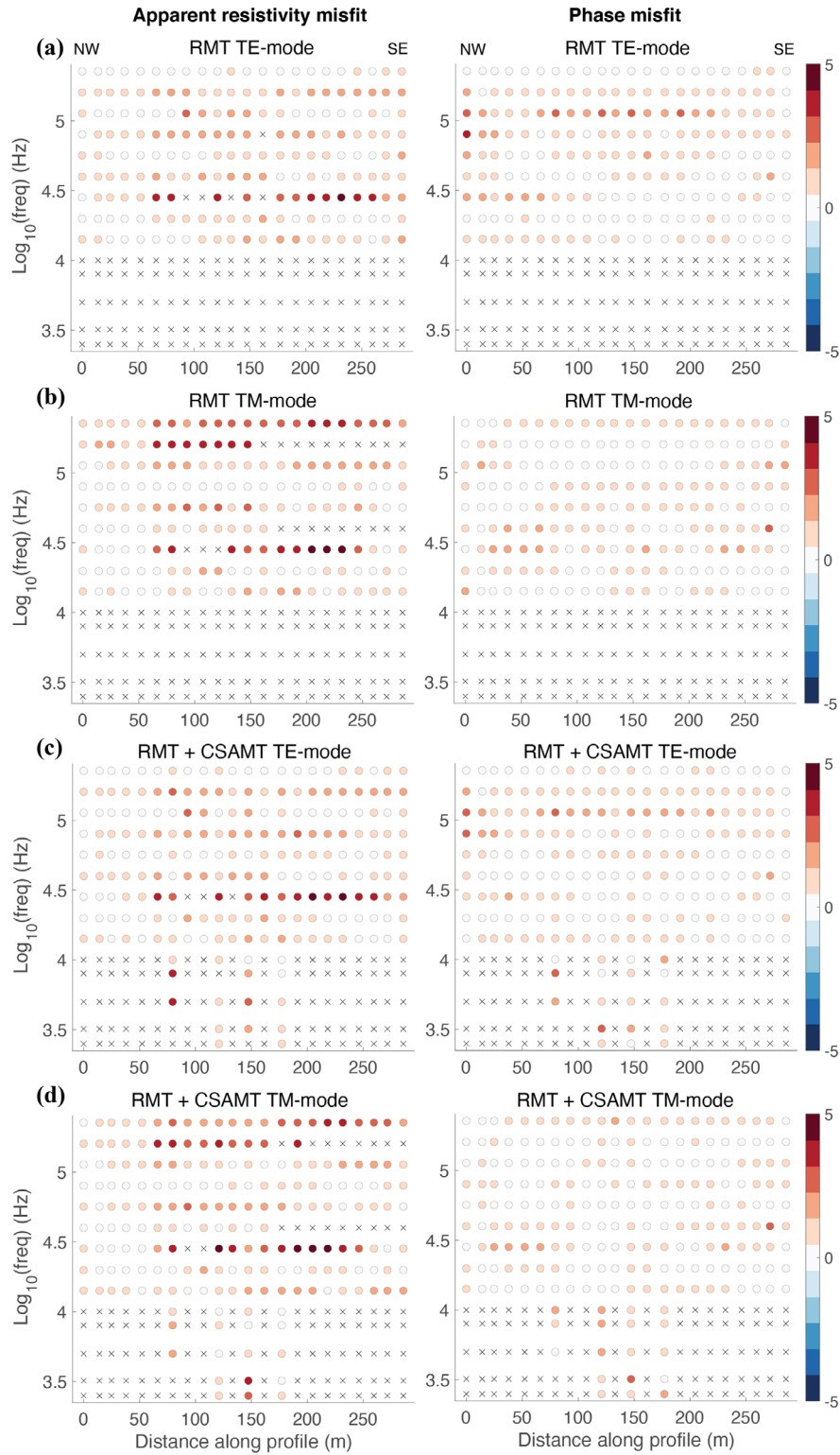
Figure 10 Data misfits corresponding the inversion in Fig. 9, which are the observed and modelled data difference normalized by the data errors. In general, phase data have lower misfits than the apparent resistivity data. The crosses mean the exclusion of data points in the corresponding inversions.

minerals within the fracture system are graphite, chlorite and calcite. The resistivity model in Figure 6(a) does not show any indication of such a lower-resistivity fracture system, which is likely because of poor data sensitivity (limited penetration depth; see in Fig. 8a–b) and partly due to smoothing imposed by the smoothness constraint used in the inversion. The new controlled-source stations make it possible to resolve the depth to bedrock in the middle of the profile, where thick lake sediments are present (Fig. 8c–d). The near-surface features interpreted in the RMT model can be observed in the new controlled-source radio-magnetotelluric (CSRMT) model as well (Fig. 6b). The locations of controlled-source stations are marked along the *x*-axis with stars. The resistivity model differs from the RMT model mainly at depth between 100–200 m along the profile, where a more resistive feature can be observed. Clearly, the sediments' lower boundary is better focused, and the fractured zone in the bedrock is detected when the controlled-source data are added. According to the borehole information, the depth to the fractured bedrock (or the bottom of lake sediments) is expected to be about 30–50 m, which seems to be better resolved with controlled-source lower frequencies. Noticeably, the resistivity of the fractured bedrock appears to be relatively low. This can be probably caused by the presence of infilling of conductive materials and clays in the fracture system.

The acquired seismic reflection data closest to the RMT profile L9 are presented in Figure 6(c). A major undulation in the seismic section (S4) can be observed (distances 150–200 m along profile) that likely marks the location where the bedrock might be eroded and can be inferred to be fractured. The CSRMT model is superimposed on the seismic section and shown in Figure 6(d). The undulations in the bedrock can be easily compared and show a clear correlation between the two datasets that have been independently processed and modelled. Based on the estimate of skin depth and the distance between the transmitter and receivers, the first controlled-source station towards the NW part of the profile might be influenced by the near-field effect (transmitter–receiver distance less than 12 times of skin depth). Since the near-field effect is more dominant at lower frequencies, the two lowest frequencies (2.5 kHz and 3.2 kHz) were omitted from the dataset prior to the inversion to eliminate effect. Sensitivities for the boundary of sediments and bedrock (anomaly A in Fig. 8) and the potential fracture zone (anomaly B in Fig. 8) are studied by model perturbation. This means that we have changed the resistivity of the model bounded in the region of anomaly A and calculated the forward response of the model and compared the data fits with the resistivity model from the

inversion shown in Figure 6(b). The resistivity of the anomalies are increased to 1000 Ωm from the inverted values. The RMS increase is the original and perturbed RMS difference normalized by the original RMS. For both anomalies, the RMS increases of combined inversions are nearly 2–3 times larger than those of RMT inversions, which indicates the increase of sensitivity at depths due to the inclusion of four CSAMT stations. Clearly, the sensitivity tests not only show the low frequency CSAMT signals increase the investigation depth of the inverse models, but also illustrate that observed data have sensitivities to the bedrock surface and potential fracture zone filled with conductive materials (Fig. 8). One should note that the most conductive deepest zone in Figure 6(b) at distances 150—200 m along the profile lies below the depth of investigation, and therefore our interpretation of the possible fracture zone (marked by white lines in Fig. 6d) is limited to depths dictated by the depth of investigation.

To further scrutinize the effectiveness of the CSRMT survey on the frozen lake, we show a comparison between the resistivity model along profile L13 and the available reflection seismic data along S6 (Fig. 9). Even though this profile is away from our most interested region, it can repeatedly demonstrated that there are improvements obtained by including the CSAMT data in the inversion. The corresponding data misfits for the inversion are shown in Figure 10. Again, phase data have lower misfits than the apparent resistivity data, and apparent resistivity data only have relatively high misfits at certain frequencies. In both the RMT and CSRMT models, the water column is perfectly resolved. However, bedrock undulation is resolved only in the CSRMT model. The resistivity of the fracture system is relatively low due to the filling of conductive materials. Penetration depth, white dashed lines in Figure 9, also shows that the discussed features are well constrained by the observed CSRMT data. We must emphasize that the smoothing regularization applied in the inversion, and the diffusive nature of electromagnetic fields in the earth, generate smoother nearly vertical low resistivity zones compared to the observed fractures in the drillholes (reported by Ignea 2015) that are much narrower and have varying dips. But, compared to the reflection seismic section, the CSRMT data still have good vertical resolution.

CONCLUSIONS

To the best of our knowledge, for the first time, controlled-source radio-magnetotelluric (CSRMT) data over a frozen lake were successfully acquired in an area close to Stockholm and in connection to the planned bypass multi-lane

underground road tunnel project. The goal was to map the depth to bedrock and investigate the presence of any fracture system, particularly in the middle of the surveyed profiles where the previously acquired boat-towed radio-magnetotelluric (RMT) dataset was incapable of resolving such details. Variation of the modelled resistivity correlates well with results reported in previous studies, available drillholes and seismic reflection data. This is also testified by a penetration depth evaluation, inversion misfit analysis and model sensitivity analysis using the model perturbation method. The quality of the CSRMT data collected is in general good, although at some stations, closer to the transmitter, the near-field effect was speculated. In a broader perspective, the idea of a CSRMT study on a f rozen lake can be used on shallow waterbodies in similar climatic conditions where only the RMT dataset is not sufficient in terms of penetration depth. A more detailed analysis can be made by 3D modelling/inversion of all densely collected RMT and CSRMT data in this survey area for future studies. We anticipate this approach to open new opportunities in the northern countries for infrastructure planning projects, where these structures are expected to cross waterbodies, and for mineral exploration where little is known about subsurface structures and bedrock. However, a Bayesian inversion could be used in the future along the full CSRMT profiles for quantitative model uncertainty studies, which is hard to achieve with deterministic inversions, such as the one we used.

ACKNOWLEDGEMENTS

DATA AVAILABILITY STATEMENT

The CSRMT data collected in this study are available for further research and can be collected by contacting the customer service at the Geological Survey of Sweden (SGU) at kundservice@sgu.se .

ORCID

Mehrdad Bastani https://orcid.org/0000-0003-3564-3754
Shunguo Wang https://orcid.org/0000-0001-6573-840X

REFERENCES

Andersson, M. and Malehmir, A. (2018) Unravelling the internal architecture of the Alnö alkaline and carbonatite complex (central Sweden) using 3D models of gravity and magnetic data. *Tectonophysics*, 740–741, 53–71.

Bastani M., Malehmir A., Ismail N., Pedersen L. B., Hedjazi F. (2009) Delineating hydrothermal stockwork copper deposits using controlled-source and radio-magnetotelluric methods: A case study from northeast Iran. *Geophysics*, 74(5), B167–B181. https://doi.org/10.1190/1.3174394

Bastani M., Hübert J., Kalscheuer T., Pedersen L. B., Godio A., Bernard J. (2012) 2D joint inversion of RMT and ERT data versus individual 3D inversion of full tensor RMT data: An example from Trecate site in Italy. *Geophysics*, 77(4), WB233–WB243. https://doi.org/10.1190/geo2011-0525.1

Bastani, M. (2001) EnviroMT – A New Controlled Source /Radio Magnetotelluric System. PhD thesis: Acta Universitatis Upsaliensis, *Uppsala Dissertations from the Faculty of Science and Technology* 32.

Bastani, M., Persson, L., Mehta, S. and Malehmir, A. (2015) Boat-towed radio-magnetotellurics (RMT) – a new technique and case study from the city of Stockholm. *Geophysics*, 80, B193–B202.

Bastani, M., Savvaidis, A., Pedersen, L.B. and Kalscheuer, T. (2011) CSRMT measurements in the frequency range of 1–250 kHz to map a normal fault in the Volvi basin, Greece. *Journal of Applied Geophysics*, 75, 180–195. https://doi.org/10.1016/j.jappgeo.2011.07.001

Constable, S.C., Parker, R.L. and Constable, C.G. (1987) Occam's inversion: a practical algorithm for generating smooth models from electromagnetic sounding data. *Geophysics*, 52(3), 289–300.

Dehghannejad M., Malehmir A., Svensson M., Lindén M., Möller H. (2017) High-resolution reflection seismic imaging for the planning of a double-train-track tunnel in the city of Varberg, southwest Sweden. *Near Surface Geophysics*, 15(3), 226–240. https://doi.org/10.3997/1873-0604.2017011

Dugan, H.A., Arcone, S.A., Obryk, M.K. and Doran, P.T. (2016) High-resolution ground-penetrating radar profiles of perennial lake ice in the McMurdo Dry Valleys, Antarctica: horizon attributes, unconformities, and subbottom penetration. *Geophysics*, 81(1), WA13–WA20. https://doi.org/10.1190/geo2015-0159.1

Dugan, H.A., Doran, P.T., Tulaczyk, S., Mikucki, J.A., Arcone, S.A., Auken, E. *et al.* (2015) Subsurface imaging reveals a confined aquifer beneath an ice-sealed Antarctic lake. *Geophysical Research Letters*, 42, 96–103. https://doi.org/10.1002/2014GL062431

Goldstein, M.A. and Strangway, D.W. (1975) Audiofrequency magnetotellurics with a grounded electric dipole source. *Geophysics*, 40, 669–683.

Huang, H. (2005) Depth of investigation for small broadband electromagnetic sensors. *Geophysics*, 70(6), G135–G142.

Ignea, S. (2015), *Major Fracture Zones in Fiskarfjärden, Stockholm*. MSc thesis, Uppsala Universitet.

Kalscheuer, T., Pedersen, L.B. and Siripunvaraporn, W. (2008) Radiomagnetotelluric two-dimensional forward and inverse modelling accounting for displacement currents. *Geophysical Journal International*, 175, 486–514. https://doi.org/10.1111/j.1365-246X.2008.03902.x

Li, X. and Pedersen, L.B. (1991) Controlled source tensor magnetotelluric. *Geophysics*, 56, 1456–1461.

Malehmir A., Zhang F., Dehghannejad M., Lundberg E., Döse C., Friberg O., Brodic B., Place J., Svensson M., Möller H. (2015) Planning of urban underground infrastructure using a broadband seismic landstreamer — Tomography results and uncertainty quantifications from a case study in southwestern Sweden. *Geophysics*, 80(6), B177–B192. https://doi.org/10.1190/geo2015-0052.1

Mehta, S., Bastani, M., Malehmir, A. and Pedersen, L.B. (2017) Resolution and sensitivity of boat-towed RMT data to delineate fracture zones–example of the Stockholm bypass multi-lane tunnel. *Journal of Applied Geophysics*, 139C, 131–143. https://doi.org/10.1016/j.jappgeo.2017.02.012.

Nilsson, P. (2008) Sjömätningar i tre passager under Mälaren, Förbifart Stockholm Teknisk Rapport Nr 2008–11, GeoNova Consulting AB, Sweden (www.geonovaconsulting.se).

Pedersen, L.B., Bastani, M. and Dynesius, L. (2005) Groundwater exploration using combined controlled-source and radiomagnetotelluric techniques. *Geophysics*, 70, G8–G15.

Pedersen, L.B., Bastani, M. and Dynesius, L. (2006) Radiotransmitters in Europe and their use in high resolution geophysical exploration of near-surface geology. *Geophysics*, 71(6), G279–G284.

Pedersen, L.B. and Engels, M. (2005) Routine 2D inversion of magnetotelluric data using the determinant of the impedance tensor. *Geophysics*, 70, 31–41.

Persson, L. (2001) Plane Wave Electromagnetic Measurements for Imaging Fracture Zones. PhD thesis. Acta Universitatis Upsaliensis, *Uppsala Dissertations from the Faculty of Science and Technology* 30.

Ronczka, M., Hellman, K., Günther, T., Wisen, R. and Dahlin, T. (2017) Electric resistivity and seismic refraction tomography: a challenging joint underwater survey at Äspö Hard Rock Laboratory. *Solid Earth*, 8, 671–682. https://doi.org/10.5194/se-8-671-2017

Spies, B.R. (1989) Depth of investigation in electromagnetic sounding methods. *Geophysics*, 54(7), 872–888.

Saraev A., Simakov A., Shlykov A., Tezkan B. (2017) Controlled source radiomagnetotellurics: A tool for near surface investigations in remote regions. *Journal of Applied Geophysics*, 146, 228–237. https://doi.org/10.1016/j.jappgeo.2017.09.017

Saraev, A., Simakov, A., Shlykov, A. and Tezkan, B. (2011) Controlled-source adiomagnetotellurics: a tool for near surface investigations in remote regions. *Journal of Applied Geophysics*, 146(2017), 228–237.

Schwamborn G. J., Dix J. K., Bull J. M., Rachold V. (2002) High-resolution seismic and ground penetrating radar-geophysical profiling of a thermokarst lake in the western Lena Delta, Northern Siberia. *Permafrost and Periglacial Processes*, 13(4), 259–269. https://doi.org/10.1002/ppp.430

Shlykov, A.A. and Saraev, A.K. (2015) Estimating the macroanisotropy of a horizontally layered section from controlled-source radiomagnetotelluric soundings. *Izvestiya, Physics of the Solid Earth*, 51(4), 583–601.

Shlykov, A., Saraev, A. and Tezkan, B. (2020) Study of a permafrost area in the northern part of Siberia using controlled source radiomagnetotellurics. *Pure and Applied Geophysics*, 177, 5845–5859. https://doi.org/10.1007/s00024-020-02621-x

Siripunvaraporn, W. and Egbert, E. (2000) An efficient data-subspace inversion method for 2D magnetotelluric data. *Geophysics*, 65, 791–803.

Streich, R. (2016) Controlled-source electromagnetic approaches for hydrocarbon exploration and monitoring on land. *Surveys in Geophysics*, 37, 47–80.

Streich, R. and Becken, M. (2010) Electromagnetic fields generated by finitelength wire sources: comparison with point dipole solutions. *Geophysical Prospecting*, 59, 361–374.

Tezkan, B., Hordt, A. and Gobashy, M. (2000) Two-dimensional radiomagnetotelluric investigation of industrial and domestic waste sites in Germany. *Journal of Applied Geophysics*, 44, 237–256.

Tezkan, B., Muttaqien, I. and Saraev, A. (2019) Mapping of buried faults using the 2D modelling of far-field controlled source radio magnetotelluric data. *Pure and Applied Geophysics*, 176, 751–766.

Turberg, P., Muller, I. and Flury, F. (1994) Hydrogeological investigation of porous environments by audiomagnetotelluric resistivity. *Journal of Applied Geophysics*, 31, 133–143.

Ugalde, H., Heureux, E.L., Lachapelle, R. and Milkereit, B. (2006) Measuring gravity on ice: an example from Wanapitei Lake, Ontario, Canada. *Geophysics*, 71(3), J23–J29. https://doi.org/10.1190/1.2189387

Wang, S., Bastani, M., Constable, S., Kalscheuer, T. and Malehmir, A. (2019) Boat-towed radio-magnetotelluric and controlled-source audio-magnetotelluric study to resolve fracture zones at Äspö Hard Rock Laboratory site, Sweden. *Geophysical Journal International*, 218(2), 1008–1031. https://doi.org/10.1093/gji/ggz162

Wang, S., Kalscheuer, T., Bastani, M., Malehmir, A., Pedersen, L.B., Dahlin, T. and Meqbel, N. (2018) Joint inversion of lake-floor electrical resistivity tomography and boat-towed radio-magnetotelluric data illustrated on synthetic data and an application from the Äspö Hard Rock Laboratory site, Sweden. *Geophysical Journal International*, 213(1), 511–533. https://doi.org/10.1093/gji/ggx414

Wannamaker, P.E. (1997) Tensor CSAMT survey over the sulphur springs thermal area, Valles Caldera, New Mexico, USA, Part II. Implications for CSAMT methodology. *Geophysics*, 62, 466–476.

Yavich, N., Malovichko, M. and Shlykov, A. (2020) Parallel simulation of audio- and radio-magnetotelluric data. *Minerals*, 10(1), 42. https://doi.org/10.3390/min10010042

Zonge, K.L. and Hughes, L.J. (1991) Controlled source audio-frequency magnetotellurics. *Electromagnetic Methods in Applied Geophysics*, V.2. Applications. Series: Investigations in Geophysics 3, 713–809.